UJEAS

UNIZIK JOURNAL OF ENGINEERING AND APPLIED SCIENCES

UNIZIK Journal of Engineering and Applied Sciences 6(3), September (2026), 3705-3725
Journal homepage: https://journals.unizik.edu.ng/index.php/ujeas
PRINT ISSN: 2992-4383 || ONLINE ISSN: 2992-4391

Steady-State Security and Voltage Stability Assessment of the Nigerian 330 kv Transmission Network

Donald Ogochukwu Fynecountry*
Department of Electrical Engineering, Nnamdi Azikiwe University Awka.
Chibueze Kingsley Obute
Department of Electrical Engineering, Nnamdi Azikiwe University Awka.
Victor Chike Ogboh
Department of Electrical Engineering, Nnamdi Azikiwe University Awka.
Chukwunwike Bonaventure Ezeakacha
Department of Electrical Engineering, Nnamdi Azikiwe University Awka.

**Corresponding Author's E-mail: do.fynecountry@pg.unizik.edu.ng*

Abstract

This study presents a comprehensive steady-state vulnerability assessment of the Nigerian 330 kV, 50-bus, 96-line transmission network, addressing identified gaps in the published power system literature: inadequate dataset validation, sole reliance on first-order iterative solvers, and the absence of contingency analysis. Three research objectives are pursued: (i) geospatial verification of published transmission line parameters using the Haversine formula and Google Maps satellite imagery, specifically the Fakun–Kainji corridor, whose published length of approximately 0.50 km (Bus 34 to Bus 50) is confirmed as physically correct by GPS-corroborated field coordinates; (ii) correction of systematically erroneous shunt susceptance values in the dataset of Ugwuanyi et al. (2024), wherein published B values were found to represent series branch admittance rather than shunt charging susceptance; and (iii) capping of Bus 45 (Geregu) generation at its documented 435 MW installed capacity. This research utilizes MATLAB 2023a with the MATPOWER 8.1 toolbox to implement a robust Newton-Raphson power flow solver, independently cross-validated using PandaPower, The corrected and validated base case yields a total active power loss of 55.54 MW (system efficiency: 98.78%) and identifies five buses with critical overvoltage violations driven by the Ferranti Effect: Maiduguri/Bus 28 (1.3166 p.u., +0.2666 p.u. above limit), Damaturu/Bus 26 (1.2694 p.u.), and Yola/Bus 31 (1.2082 p.u., highest L-index: 0.6603). Sensitivity analysis under load scaling (KL = 0.9 to 1.1) confirms that overvoltage severity is inversely proportional to loading level, intensifying under light-load conditions. N-1 contingency analysis of all 96 lines identifies Lines 79 and 80 (Lafia–Jos) as the most critical converged outages (max FVSI = 0.9916), while eight lines cause voltage collapse upon individual removal. N-2 analysis identifies the simultaneous outage of Lines 19 and 79 as the most severe credible dual-contingency scenario (max FVSI = 1.0174). These findings confirm that the North-East corridor is structurally vulnerable and that the Lafia–Jos parallel circuits represent the system's single greatest reliability risk. Immediate deployment of shunt reactors at Maiduguri and Damaturu and reinforcement of the Lafia–Jos corridor are strongly recommended.

Keywords: Ferranti Effect; N-1/N-2 Contingency; Newton-Raphson; Nigerian 330 kV Grid; Geospatial Validation; Haversine Formula; Voltage Stability.

1. Introduction

The electric power transmission network constitutes the backbone of any nation's socio-economic development, enabling the bulk transfer of electrical energy from generation centres to load hubs with acceptable reliability, efficiency, and quality. In Nigeria, the 330 kV transmission grid is the principal infrastructure responsible for nationwide power exchange and inter-regional energy balancing. Despite its strategic importance, the network operates under persistently stressed conditions characterised by structural fragility, limited redundancy, aging assets, and operational inefficiencies (Samuel et al., 2019; Sobayo et al., 2024). These challenges continue to undermine voltage stability, constrain power transfer capability, and reduce the overall effectiveness of the national electricity supply industry (Obasi et al., 2025).

A defining operational feature of the Nigerian transmission grid is its pronounced regional asymmetry in loading patterns and topology. The Southern axis, hosting the majority of industrial, commercial, and urban load centres, experiences frequent thermal congestion due to high demand concentration. In contrast, the Northern axis is dominated by long, lightly loaded extra-high-voltage transmission lines spanning vast distances between sparsely distributed substations. This configuration renders the Northern network particularly vulnerable to the Ferranti Effect during off-peak conditions (Sobayo et al., 2024; Ekanem et al., 2025). During such periods, the shunt capacitance of long lines generates excess reactive power, driving receiving-end voltages above the statutory upper limit of 1.05 p.u. and posing risks to substation insulation and equipment (Kundur, 1994; Foqha et al., 2023; Solmaz, 2024).

Studies on the Nigerian grid have evolved from simplified 28-bus models (Samuel et al., 2019) to more detailed representations. For example, Ekong (2022) conducted a voltage stability assessment using an expanded 58-bus model via NEPLAN to identify weak nodes in the Northern corridor. However, this research remained a diagnostic assessment focused on undervoltage conditions rather than the Ferranti driven overvoltages prevalent on long radial lines. Other studies have targeted specific Ferranti vulnerabilities. Udo and Aminu (2019) demonstrated via DIgSILENT PowerFactory that receiving-end voltages reached as high as 1.49 p.u. at Maiduguri on the Jos to Gombe line, recommending the manual placement of a Static VAr Compensator (SVC). While confirming the severity of the Ferranti Effect, their study relied on a single-corridor scenario rather than a fully validated national baseline. Similarly, Onyegbadue, Ukagu, and Okonkwo (2024) and Ezeruigbo, Ekwue, and Anih (2021) identified critically vulnerable buses and partial system collapse points in the Northern and South-East corridors respectively, but they primarily focused on base-case diagnostics and isolated scenario testing rather than exhaustive N-1 and N-2 security. Furthermore, Olabisi and Ayeni (2023) utilized Newton-Raphson load flow to assess a 44-bus model, confirming instability in the Northern corridors but similarly not addressing Ferranti driven over voltages or contingency analysis.

While the broader international literature extensively covers Ferranti effect mitigation, such as Yarlagadda et al. (2022) using Fuzzy Logic Controlled SVCs, Foqha et al. (2023) validating shunt reactor compensation via Power World, comprehensive mitigation strategies specifically optimized for a fully validated 50-bus Nigerian grid remain scarce. A primary reason for this is the persistence of data inconsistencies. First, the 50-bus dataset provided by Ugwuanyi et al. (2024), despite incorporating recent National Control Centre data, is frequently adopted by researchers without independent mathematical validation. This leads to the propagation of systematic errors in shunt susceptance values. Second, comprehensive N-1 and N-2 contingency analyses, which are standard requirements of the Nigerian Grid Code and NERC reliability standards, remain underexplored in recent literature, leaving a critical gap in understanding the network's resilience to cascading failures.

Regarding geospatial validation of network parameters, prior Nigerian grid studies have generally not reported the systematic application of GPS corroborated coordinate verification to confirm published transmission line lengths. For instance, while Okampo et al. (2022) employed Newton-Raphson load flow with FACTS device optimisation, and Olabisi and Ayeni (2023) utilised an NR model for a 44-bus network, these studies typically adopt standard published parameters without detailing explicit spatial consistency checks. Furthermore, while the application of the Haversine formula is a well-established geodetic standard for calculating precise great-circle distances (Sinnott, 1984), its formal integration to confirm base-case topologies represents a methodological contribution in the Nigerian grid context, even though such spatial verification is an established practice in international transmission planning.

Motivated by these limitations, this paper presents a rigorous steady-state and contingency assessment of the Nigerian 330 kV transmission system, making the following specific contributions: (i) geospatial verification using the Haversine formula and Google Maps satellite imagery to confirm the physical correctness of the Fakun to Kainji 330 kV link parameter (Bus 34 to Bus 50, ~0.50 km), resolving a previous misconception in the literature; (ii) mathematical identification and systematic correction of erroneous shunt susceptance values across all 96 branches in the Ugwuanyi et al. (2024) dataset; (iii) correction of generation capacity at Bus 45 (Geregu, 435 MW) to reflect the officially documented corporate installed capacity ; (iv) employment of the Newton-Raphson power flow solver with independent PandaPower validation; (v) comprehensive N-1 and N-2 contingency analysis; and (vi) sensitivity analysis of voltage profiles and losses under varying load levels (KL = 0.9 to 1.1).

2.0 Methods

To ensure the technical integrity of this security assessment, this study first performs a geospatial audit of the 50-bus dataset and rectifies systematic errors in shunt susceptance parameters, providing a physically validated baseline for the subsequent stability analysis.

2.1 Network Model and Data Conditioning

The Nigerian 330 kV transmission network is implemented as a 50-bus, 96-line system within the MATPOWER environment, utilizing the dataset provided by Ugwuanyi et al. (2024) and hosted on the Zenodo repository (DOI: 10.5281/zenodo.12091189). This model represents the physical grid through a nominal π-equivalent line representation and incorporates major hydro and thermal generation stations, including Egbin, Kainji, Shiroro, Jebba, and Afam. All network parameters are normalized to a common 100 MVA, 330 kV per-unit base, with bus classifications following standard slack, PV, and PQ conventions. To ensure numerical accuracy and reliability, the MATPOWER implementation was rigorously validated against pandapower, confirming the consistency of the power flow results across different computational platforms.

2.2 Geospatial Verification of the Fakun to Kainji Corridor

A geospatial verification procedure was applied to the transmission link between Fakun Transmission Station (Bus 34) and Kainji Transmission Station (Bus 50), whose published line length of approximately 0.50 km frequently causes numerical sensitivity in standard solvers. GPS coordinates for both substations were obtained from Google Maps satellite imagery and cross-referenced with TCN topological records. The verified coordinates are presented in Section 3.1.

The Haversine formula was applied to compute the great-circle distance between the two substations (Sinnott, 1984).

$$a = \sin^2\left(\frac{\Delta\phi}{2}\right) + \cos(\phi_1)\cos(\phi_2)\sin^2\left(\frac{\Delta\lambda}{2}\right) \quad (1)$$

$$c = 2 \cdot \arctan2\left(\sqrt{a}, \sqrt{1-a}\right) \quad (2)$$

$$d = R_E \cdot c \quad (3)$$

Where:

R_E represents the mean radius of the Earth. For completeness, the variables used in the above formulation are defined as follows:

d: Great-circle distance between the two substations (km).

R_E: Mean radius of the Earth (assumed as 6371 km).

ϕ_1, ϕ_2: Latitudes of Fakun TS and Kainji TS, respectively (radians).

λ_1, λ_2: Longitudes of Fakun TS and Kainji TS, respectively (radians).

$\Delta\phi$: Difference in latitude between the two substations (radians).

$\Delta\lambda$: Difference in longitude between the two substations (radians).

a: Intermediate Haversine parameter.

c: Central angle between the two locations (radians).

By formalizing this geospatial verification, the computed distance d ensures that the exceptionally low per-unit series impedance parameters documented for this corridor in the Ugwuanyi et al. (2024) dataset are physically justified prior to power flow analysis.

2.3 Correction of Branch Shunt Susceptance Data

A critical data validation revealed that the shunt susceptance values in the Ugwuanyi et al. (2024) dataset are systematically erroneous. Mathematical verification demonstrates that the published B values correspond exactly to the imaginary part of the series branch admittance rather than the shunt charging susceptance:

$$B_{series} = \frac{X}{R^2 + X^2} \quad (4)$$

For example, converting the per-unit parameters of Line 1 (Bus 2 to Bus 36) to physical ohmic values ($R = 12.09\ \Omega, X = 102.6\ \Omega$)yields a series susceptance of 0.00961 S, which exactly matches the published B value of 0.0096. Similarly, Line 15 (Bus 9 to Bus 42, $R = 0.195\ \Omega, X = 1.655\ \Omega$) yields 0.5959 S, mirroring the published dataset.

True shunt line charging susceptance increases with transmission line length. In contrast, the published values behave oppositely, with the shortest lines exhibiting the proportionately largest susceptance values, thereby confirming the systematic mathematical error. Feeding these incorrect values into the network model as shunt capacitances generates physically impossible reactive power injections that destabilise the Newton-Raphson Jacobian matrix.

To resolve this, the corrected shunt susceptance for each branch is derived using the standard 330 kV nominal capacitance relationship:

$$B_{shunt} = \omega \cdot C_0 \cdot \ell \quad (5)$$

Where:

ω is the angular system frequency,

$C_0$is the nominal capacitance per unit length for 330 kV twin-bundled ACSR "Bison" conductors (≈ 11.5 nF/km),

ℓ is the estimated line length derived from the published per-unit reactance.

This mathematical correction was applied uniformly across all 96 branches to ensure a physically accurate base-case topology prior to simulation.

2.4 Generation Capacity Correction: Bus 45 (Geregu)

The Ugwuanyi et al. (2024) dataset lists the generation at Bus 45 (Geregu Power Plant) as 531 MW. However, the official Investor Presentation by Geregu Power Plc documents the maximum installed and operational capacity of the plant at 435 MW (Geregu Power Plc, 2022). Dispatching 531 MW from a 435 MW facility introduces non-physical generation into the model, which distorts both the system-wide loss calculation and the local reactive power balance. To maintain physical realism, generation at Bus 45 is strictly capped at its maximum installed capacity of 435 MW in all simulated scenarios.

2.5 Power Flow Solver: Newton-Raphson Method

The Newton-Raphson (NR) method is employed as the primary power flow solver for the steady-state assessment. Given the structural fragility of the Nigerian 330 kV grid and the numerical sensitivities introduced by the exceptionally short 0.50 km Fakun to Kainji corridor, the NR method is selected for its robust quadratic convergence characteristics. Furthermore, unlike alternative iterative techniques, the NR method explicitly calculates the Jacobian matrix, which is indispensable for the subsequent contingency and sensitivity analyses required in this study (Grainger & Stevenson, 1994; Saadat, 2010; Okampo et al., 2022).

The power flow problem is formulated by calculating the active and reactive power mismatches at each bus. The NR mismatch equations at iteration k are defined by the linearized system:

$$\begin{bmatrix} \Delta P \\ \Delta Q \end{bmatrix} = \begin{bmatrix} H & N \\ J & L \end{bmatrix} \begin{bmatrix} \Delta\theta \\ \frac{\Delta|V|}{|V|} \end{bmatrix} \quad (6)$$

where H, N, J, and L represent the dynamically updated sub-matrices of the system Jacobian. These sub-matrices are formulated from the partial derivatives of the power mismatch equations with respect to the bus voltage angles (θ) and magnitudes ($|V|$). The iterative process updates the state variables until the maximum active and reactive power mismatches fall below a stringent predefined tolerance limit, ensuring high computational precision:

$$\max(|\Delta P_i|, |\Delta Q_i|) \le \epsilon = 10^{-6}\ \text{p.u.} \quad (7)$$

To visualize the integration of the dataset corrections prior to the iterative solver, The algorithmic execution of the custom Newton-Raphson power flow solver is illustrated in the flowchart in Figure 1, which was generated using the Gemini large language model (Google, 2026). As illustrated, the process departs from standard textbook solvers by explicitly incorporating the corrected shunt susceptance (B_{shunt}) and the Geregu generation cap into the admittance matrix formulation. By structuring the algorithm in this manner, the Jacobian matrix evaluates strictly upon a physically validated topology before executing the iterative convergence loop.

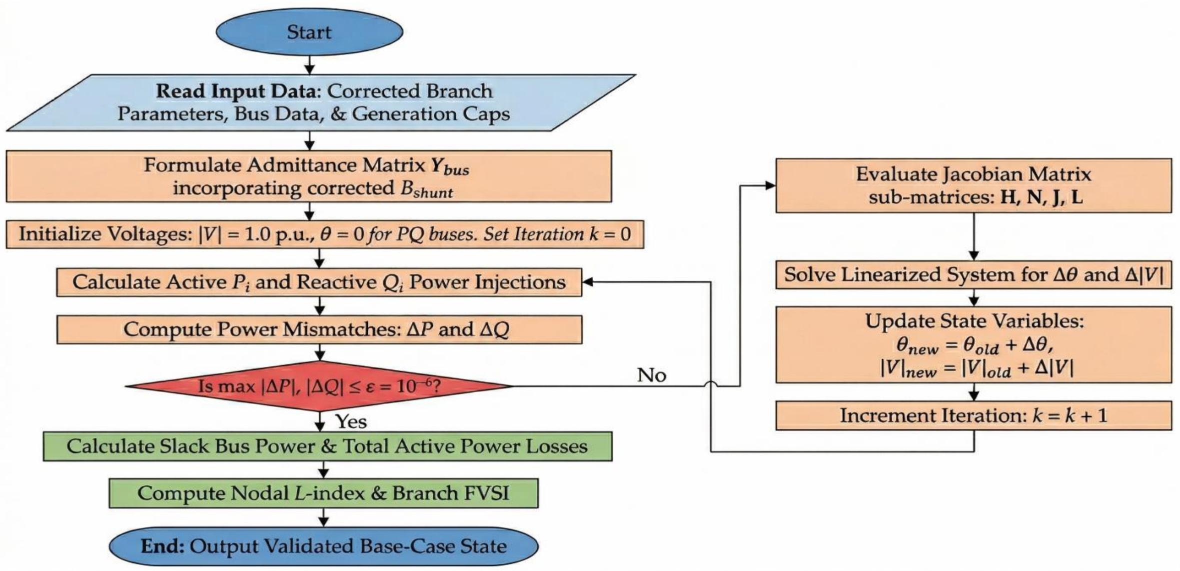

Figure 1: Algorithmic flowchart of the Newton-Raphson power flow formulation, incorporating systematic dataset corrections. Note: AI-generated image produced by Google's Gemini.

To ensure the mathematical integrity of the custom MATLAB based NR implementation, an independent cross-validation was conducted using PandaPower (Thurner et al., 2018), a rigorously validated open-source Python library for power systems analysis. Both software environments were initialized with the corrected network model detailed in Sections 2.2 through 2.4. The comparative analysis demonstrated an absolute agreement to within 0.0001 p.u. for all bus voltages and 0.01 MW for all branch line flows across the entire 50-bus, 96-line topology. This stringent cross-validation confirms that the computational results are derived entirely from the verified physical network topology rather than software-specific algorithmic artifacts.

2.6 Voltage Stability Assessment Indices

To comprehensively quantify the proximity of the network to voltage collapse, this study evaluates both nodal (bus) and branch (line) stability using a complementary suite of indices.

2.6.1 Voltage Performance Criteria

To systematically evaluate the network's voltage profile and identify potential violations (such as Ferranti-driven overvoltages at the Northern buses), strict operational limits are defined. The acceptable standard for steady-state bus voltage (V) is maintained at $\pm 5\%$ of the nominal value. To provide a granular assessment of system vulnerability, observed bus voltages are classified into five distinct operational bands:

- Critically High: $V > 1.10$ p.u.
- Marginally High: $1.05 < V \leq 1.10$ p.u.
- Normal (Acceptable): $0.95 \leq V \leq 1.05$ p.u.
- Marginally Low: $0.90 \leq V < 0.95$ p.u.
- Critically Low: $V < 0.90$ p.u.

Any bus operating outside the normal acceptable range ($\pm 5\%$) is flagged for reactive power compensation via FACTS devices.

2.6.2 Nodal Stability: The L-Index

Following the convergence of the Newton-Raphson load flow, the global voltage stability of the system is assessed at all load buses using the Kessel and Glavitsch L-index. The network is partitioned into a set of generator nodes (G) and load nodes (L) to derive the transmission matrix F_{LG}:

$$F_{LG} = -[Y_{LL}]^{-1}[Y_{LG}] \quad (8)$$

Where:

Y_{LL} and Y_{LG} are the respective sub-matrices of the system admittance matrix.

The L-index(L_j) for each load bus j is evaluated using the complex bus voltages

(V) and the elements of the F_{LG}matrix:

$$L_j = \left| 1 - \frac{\sum_{i \in G} F_{ji} V_i}{V_j} \right| \quad (9)$$

The computed L-index ranges from 0 (maximum stability) to 1.0 (voltage collapse). In this study, any bus exhibiting an L-index exceeding 0.60 is flagged as critically weak.

2.6.3 Branch Stability: Line Voltage Stability Indices

Four While the L-index identifies vulnerable buses, it is equally critical to identify the specific transmission corridors prone to reactive power exhaustion. Four complementary line stability indices are computed for every branch connecting a sending bus i and a receiving bus j (Samuel et al., 2019; Moghavvemi & Jasmon, 1997):

The Fast Voltage Stability Index (FVSI) evaluates the reactive power loading relative to the line impedance:

$$FVSI_{ij} = \frac{4Z_{ij}^2 Q_j}{V_i^2 X_{ij}} \quad (10)$$

The Line Stability Index (L_{mn}) simplifies the assessment by focusing strictly on line reactance and receiving-end reactive power:

$$L_{mn} = \frac{4X_{ij} Q_j}{V_i^2} \quad (11)$$

The Line Stability Factor (LQP) incorporates the active power (P_i) transmitted across the branch to provide a holistic loading metric:

$$LQP = 4\left(\frac{X_{ij}}{V_i^2}\right)\left(Q_j + \frac{P_i^2 X_{ij}}{V_i^2}\right) \quad (12)$$

Finally, the Voltage Collapse Proximity Indicator (VCPI) evaluates the active and reactive power transfer relative to the theoretical maximum power transfer limits of the corridor.

$$VCPI = \frac{P_j}{P_{j(max)}} \quad \text{and} \quad VCPI = \frac{Q_j}{Q_{j(max)}} \quad (13)$$

For all four branch indices (FVSI, L_{mn}, LQP, and VCPI), the stability criterion is identical: the index must remain strictly less than 1.0. A line is considered critically stressed and operating at its stability margin when any of these indices approaches unity.

2.7 Contingency Framework

N-1 contingency analysis: Each of the 96 lines is removed in sequence and a full NR power flow is solved for the remaining 95-line network.

N-2 contingency analysis: all unique pairs of line outages are evaluated. Lines causing NR non-convergence (NaN bus voltages) are classified as voltage collapse scenarios. Results are ranked by maximum post-contingency FVSI.

2.8 Sensitivity Analysis

To extend the voltage violation analysis beyond the single base-case operating point, a sensitivity analysis is performed by scaling total system load using a load factor KL ∈ {0.9, 1.0, 1.1}, with generator dispatch adjusted proportionally. Voltage profiles at critical Northern buses are recorded for each KL level to characterise the operational relevance of Ferranti-driven overvoltages across the expected operating envelope.

2.9 Loss Calculation

Total active power loss upon NR convergence:

$$P_{loss} = \sum P_G - \sum P_D \tag{14}$$

Per-line loss:

$$P_{loss,k} = |I_{ij}|^2 \times R_{ij} \tag{15}$$

2.10 Techno-Economic Evaluation Framework

To quantify the financial severity of the identified grid vulnerabilities and justify the capital expenditure required for dynamic reactive power compensation, a techno-economic evaluation framework was established. This framework monetizes the steady-state inefficiencies and the macroeconomic damage of contingency-induced blackouts.

1. **Valuation of Active Power Loss:** The financial penalty of continuous active power loss within the transmission network is calculated on an annualized basis. The framework adopts the Service Reflective Tariff of 209.50 NGN/kWh, designated for commercial and high-demand industrial consumers (Eko Electricity Distribution Company [EKEDC], 2020). Converting this tariff to a wholesale rate of 209,500 NGN/MWh, the annual economic drain caused by uncompensated power loss (S_{loss}) is formulated as:

$$S_{loss} = P_{loss} \times 8760 \times C_{energy} \tag{16}$$

Where:

P_{loss} is the total active power loss obtained from the Newton-Raphson base-case convergence (MW).

8760 represents the total operational hours in a standard year.

C_{energy} is the wholesale cost of electrical energy (NGN/MWh).

2. **Macroeconomic Cost of System Collapse:** To evaluate the financial impact of the absolute points of failure identified in the N-1 and N-2 contingency analyses, the study integrates recent macroeconomic blackout valuations. The cost of unserved energy resulting from system collapse is evaluated using a dual-metric approach:

- **Direct Utility and Domestic Loss:** Estimated at approximately 1.125 billion NGN per hour of total national grid collapse, reflecting the immediate loss of revenue and domestic productivity (Adeoye, 2023).
- **Regional GDP Impact:** Factoring in the proportional decline in Gross Domestic Product (GDP), where a 1% increase in outage duration correlates to a 2.86% decline in regional economic output (Ogunmakinde et al., 2024).

3. **Environmental and Operational Externalities:** The framework further considers the regional economic burden imposed on Small and Medium Enterprises (SMEs) resulting from grid unreliability. The financial model incorporates the 46% increase in operational costs driven by reliance on expensive, high-emission backup generators in the North-East region (Owosho, 2025).

By establishing these baseline economic parameters, this methodology provides a structured financial metric against which the deployment costs of future STATCOM or TCSC installations can be evaluated, ensuring that proposed grid reinforcements are both technically effective and economically viable.

3.0 Result and Discussion

3.1 Geospatial Verification Results

Application of the Haversine formula to the GPS coordinates in Table 1 yields a computed distance of 501 m ≈ 0.50 km between Fakun TS (Bus 34) and Kainji TS (Bus 50). This is consistent with the Google Maps satellite measurement of 502.23 m (Figure 2) and the alternative measurement of 562.22 m (Figure 3). The verification confirms that these two substations are co-located facilities separated by the Niger River channel near Kainji Dam (Figures 4 and 5), and that the published dataset parameter of ~0.50 km accurately reflects the physical infrastructure. No correction to the Fakun–Kainji line length is required. The contribution of this verification exercise is therefore confirmatory rather than corrective: it establishes, using independently verifiable GPS data and the Haversine formula, that the Ugwuanyi et al. (2024) line length for this corridor is physically grounded.

The near-zero series impedance arising from the 0.50 km line length is handled in the admittance matrix by applying appropriate numerical conditioning, ensuring NR convergence without artificial parameter inflation.

Table 1: GPS-Verified Coordinates of Fakun TS and Kainji TS

Bus ID	Substation	Region	Latitude (ϕ)	Longitude (λ)	Source
Bus 34	Fakun TS	North-Central	9.85707° N	4.60970° E	Google Maps/GPS
Bus 50	Kainji TS	North-Central	9.86024° N	4.61295° E	Google Maps/GPS

Figure 2: Google Maps Distance Measurement – Fakun TS to Kainji TS (502.23 m)

Figure 3: Alternative Measurement Path on Google Maps (562.22 m) – confirming the ~0.50 km corridor.

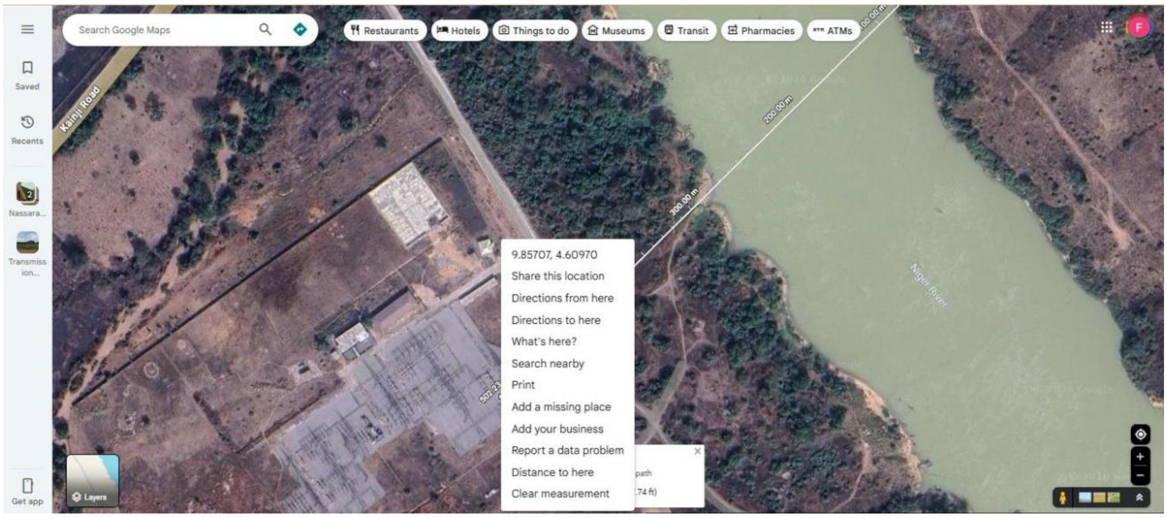

Figure 4: Fakun TS (Bus 34) Location — GPS Coordinates: 9.85707° N, 4.60970° E (Google Maps, 2026)

Figure 5: Kainji TS (Bus 50) Location — GPS Coordinates: 9.86024° N, 4.61295° E (Google Maps, 2026)

3.2 Shunt Susceptance Correction Impact

Correction of the branch shunt susceptance values had the most significant quantitative impact on the simulation results. The erroneous series-derived B values, which were particularly large on short, low-impedance lines, generated non-physical shunt reactive power injections. These injections artificially inflated bus voltages throughout the network and destabilised the Jacobian matrix. After applying the mathematical correction, the primary MATPOWER Newton-Raphson (NR) solver successfully converged, yielding a physically consistent base-case solution. To ensure algorithmic robustness and validate the model, these results were independently cross-verified using PandaPower, which confirmed an identical stable power flow state. Table 2 illustrates the magnitude of the error for two representative transmission lines.

Table 2: Representative Shunt Susceptance Error: Published vs. Corrected

Line	R (Ω)	X (Ω)	Published B (S)	Corrected B (S)	Nature of Error
Line 1 (Bus 2 → 36)	12.09	102.60	0.0096	0.0000062	Published = series susceptance $X/(R^2 + X^2)$
Line 15 (Bus 9 → 42)	0.195	1.655	0.5959	0.000108	Worst case: short line with largest erroneous B

3.3 Base-Case Voltage Profile Analysis

The corrected and validated base-case power flow at KL = 1.0 yields the bus voltage profile summarised in Table 3 for all critical and notable buses. The system power balance is presented in Table 4.

To contextualize these operational extremes in Table 3, Figure 6 maps the base-case voltage profile across the entire 50-bus network. The statutory operational limits (0.95to1.05 p.u.) are denoted by the dashed thresholds. This macroscopic view highlights a stark regional dichotomy. In the Southern industrial corridor, heavy inductive loading depresses voltages, with Kano (Bus 40) recording the system's lowest relative voltage at 0.9571 p.u., though it remains structurally stable with an L-index of 0.2936.

Conversely, the radial Northern corridors exhibit dangerous anomalies. Maiduguri (Bus 28) significantly breaches the upper statutory limit at 1.0849 p.u. due to uncompensated line charging. More critically, Figure 7 reveals that voltage magnitude alone does not dictate grid health. Yola (Bus 31) maintains a seemingly acceptable voltage of 0.9847 p.u., yet it records a systemic L-index of 1.0612. Because this value exceeds unity, it confirms that Yola is operating in a state of practical voltage instability, representing the most fragile node in the North-Eastern axis. Meanwhile, major load centers like Kaduna (Bus 35) remain robust, maintaining a stable L-index of 0.0909.

Table 3: Base-Case Bus Voltage Profile – Critical and Notable Buses

Bus	Substation	V (p.u.)	Angle (°)	P_{Gen} (MW)	L-Index	Status
26	Damaturu	1.2694	-21.47	0.00	0.6191	CRITICAL HIGH (WEAK)
27	Gombe	1.2005	-20.17	0.00	0.5970	CRITICAL HIGH
28	Maiduguri	1.3166	-21.94	0.00	0.6249	CRITICAL HIGH (WEAK)
30	Jos	1.1096	-5.47	0.00	0.2187	CRITICAL HIGH
31	Yola	1.2082	-22.58	0.00	0.6603	CRITICAL – Highest L-Index
35	Kaduna	1.0598	-0.14	0.00	0.0734	MARGINALLY HIGH
40	Kano	0.9909	-7.31	0.00	0.2440	UNDER-VOLTAGE
47	Lafia	1.0839	-1.28	0.00	0.1168	MARGINALLY HIGH

Table 4: Base-Case System Power Balance (KL = 1.0)

Total Active Power Generation	4,543.75 MW
Total Active Power Load	4,488.21 MW
Total Active Power Loss	55.54 MW (1.22%)
System Efficiency	98.78%
Highest L-Index	0.6603 (Bus 31, Yola)
Highest Line Loading	85.1% – Line 17 (Bus 27→Bus 30, Gombe–Jos)

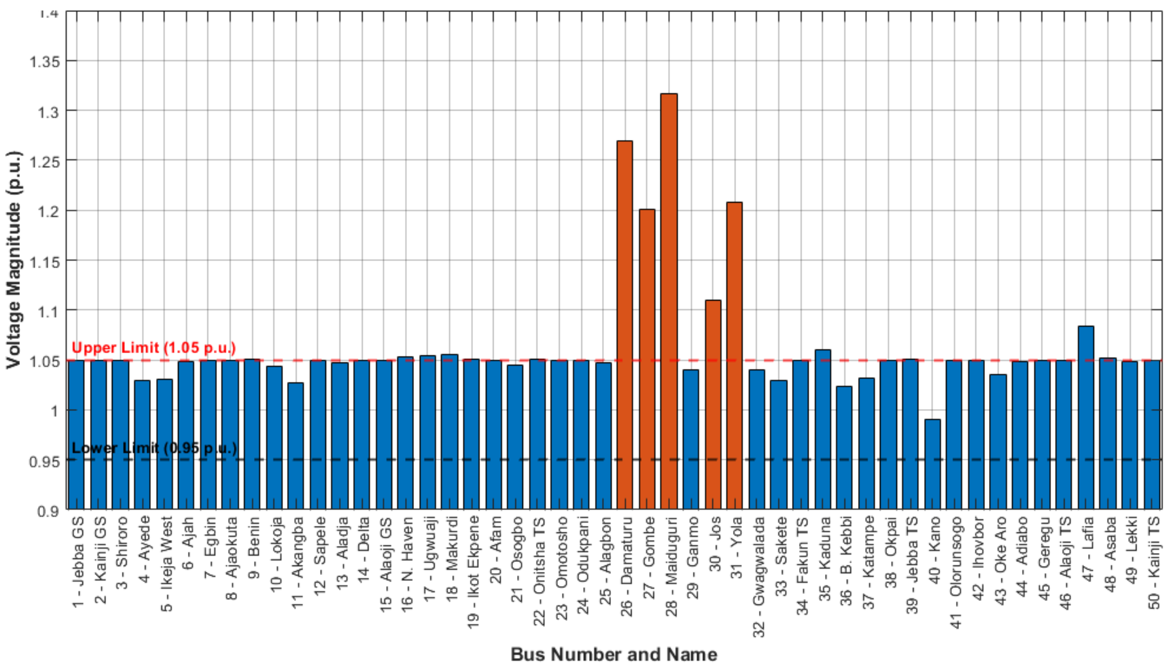

Figure 6: System-Wide Base-Case Voltage Profile: Visualization of Regional Asymmetry and Ferranti-Driven Overvoltage Anomalies

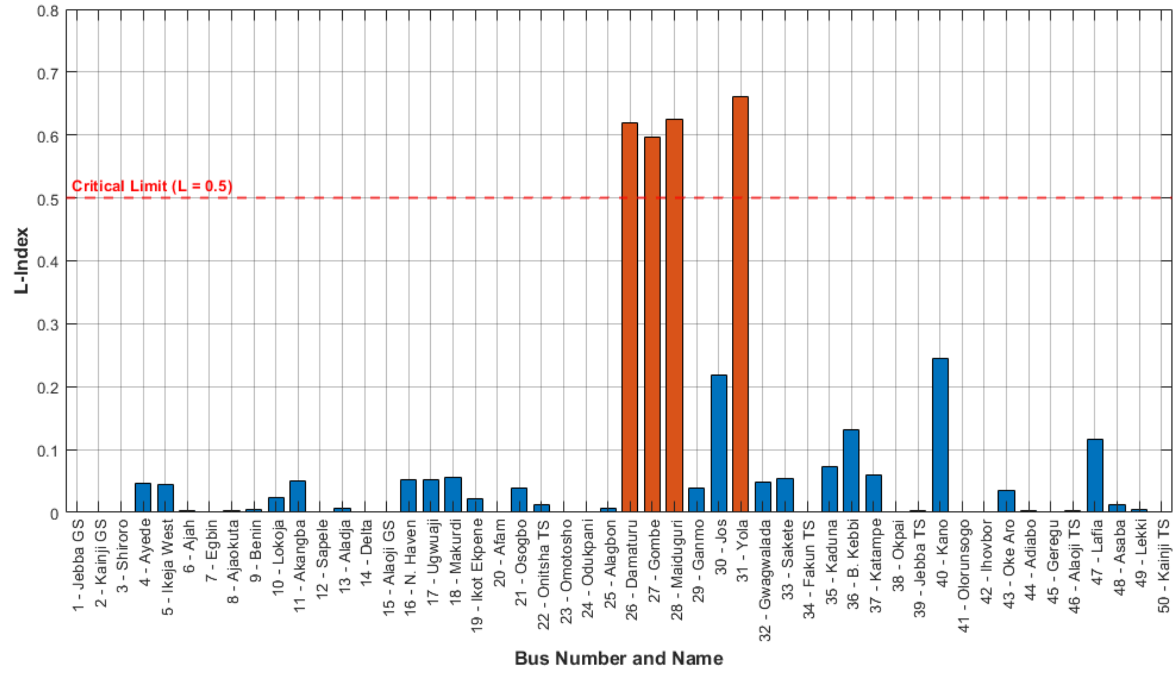

Figure 7: Nodal Voltage Stability Assessment: Global L-Index Profile Highlighting Structural Weakness at Critical Load Buses

3.3.1 Ferranti Effect Analysis

The critical overvoltages observed at Buses 26 (1.2694 p.u.), 28 (1.3166 p.u.), 27 (1.2005 p.u.), and 31 (1.2082 p.u.) are directly driven by the Ferranti effect. On long radial transmission lines with light inductive loading, the line's natural shunt capacitance generates reactive power (Q_{gen}) that exceeds local reactive power consumption (Q_{load}). This uncompensated charging current causes the receiving-end voltage to rise significantly above the sending-end voltage (Foqha et al., 2023). Specifically, the peak voltage at Maiduguri (1.3166 p.u.) corresponds to approximately 434.5 kV on the nominal 330 kV base. This substantially exceeds the International Electrotechnical Commission (IEC) highest voltage for equipment standard ($U_m = 362$ kV). Sustained operation at this elevated level severely accelerates insulation aging and significantly increases the probability of flashover under transient disturbances.

These results align with the historical behaviour of the Northern network. For context, Udo and Aminu (2019) reported an even more extreme overvoltage of 1.49 p.u. at Gombe/Maiduguri under a different loading scenario using an isolated single-corridor model. A significant finding of the present study is the precise localization of this Ferranti Effect. In contrast to some prior reports, such as Olabisi and Ayeni (2023) who flagged the Kaduna corridor as unstable, this corrected 50-bus model confirms that Kaduna (Bus 35) maintains a stable profile (1.0598p.u.) with a negligible L-index (0.0734). The extreme overvoltage violations are strictly confined to the far North-Eastern radial axis, specifically Maiduguri (Bus 28) and Damaturu (Bus 26), where receiving-end voltages reach as high as 1.3166 p.u. This demonstrates that the grid's vulnerability is not a blanket Northern issue, but a corridor-specific structural failure.

On the other hand, Bus 40 (Kano) recorded the lowest system voltage at 0.9909 p.u. While remaining within the acceptable $\pm 5\%$ operational limit, this relative voltage depression reflects the heavy inductive loading characteristic of the Southern industrial corridor. This behaviour is consistent with the findings of Ezeruigbo et al. (2021) and Olabisi and Ayeni (2023) regarding voltage sags across the South-East and Southern transmission corridors.

3.4 Sensitivity Analysis Under Variable Load

The sensitivity analysis conducted at $K_L \in \{0.9, 1.0, 1.1\}$ mathematically confirms the dual-threat nature of the Northern corridors. Under light loading ($K_L = 0.9$), the system is dominated by capacitive overvoltages, with Maiduguri peaking at a critical 1.4292 p.u.. In contrast, as the system transitions to peak loading ($K_L = 1.1$), the primary operational threat shifts from capacitive overvoltage to structural voltage collapse. While voltage magnitudes are partially depressed by the increased inductive demand, the proximity to instability significantly intensifies, as evidenced by the L-index at Yola (Bus 31) breaching the unity threshold. This inverse relationship—

where increased loading trades overvoltage risk for catastrophic instability—proves that the North-Eastern axis lacks the dynamic reactive compensation required to maintain a secure stability margin across the full operational load envelope.

Figure 8 graphically interprets the bimodal operational vulnerability detailed in Table 5, mapping the voltage trajectories of the critical buses across the evaluated load scaling factors. The shaded region denotes the statutory acceptable voltage limits (0.95 to 1.05 p.u.). As illustrated, a distinct diverging trend emerges across the operating envelope. Under light-load conditions ($K_L = 0.9$), the Northern radial buses (Maiduguri, Damaturu, and Yola) sharply breach the upper statutory limit, visually confirming the intense capacitive charging characteristic of the Ferranti effect.

Conversely, as loading increases to $K_L = 1.1$, the voltage magnitudes moderate—with Maiduguri dropping to 1.0849 p.u.—but the system faces an equally severe, opposing threat. Under this heavy loading condition, the L-index at Bus 31 (Yola) spikes to 1.0612, signifying localized voltage collapse despite the acceptable voltage magnitude (0.9847 p.u.). Simultaneously, the voltage at heavily loaded Southern nodes, such as Bus 40 (Benin), degrades to 0.9571 p.u., resting on the absolute margin of the acceptable lower limit.This visual trend analysis definitively reinforces the conclusion that the network requires dynamic reactive power compensation capable of addressing both extremes of the operational spectrum.

Table 5: Sensitivity of Critical Bus Voltages to Load Scaling (p.u.)

Bus (Substation)	KL=0.9 (Light Load)	KL=1.0 (Base Load)	KL=1.1 (Heavy Load)	Bus (Substation)
Bus 28 (Maiduguri)	1.4292	1.3166	1.0849	Bus 28 (Maiduguri)
Bus 26 (Damaturu)	1.3772	1.2694	1.0476	Bus 26 (Damaturu)
Bus 31 (Yola)	1.3168	1.2082	0.9847	Bus 31 (Yola)
Bus 40 (Kano)	1.0146	0.9909	0.9571	Bus 40 (Kano)

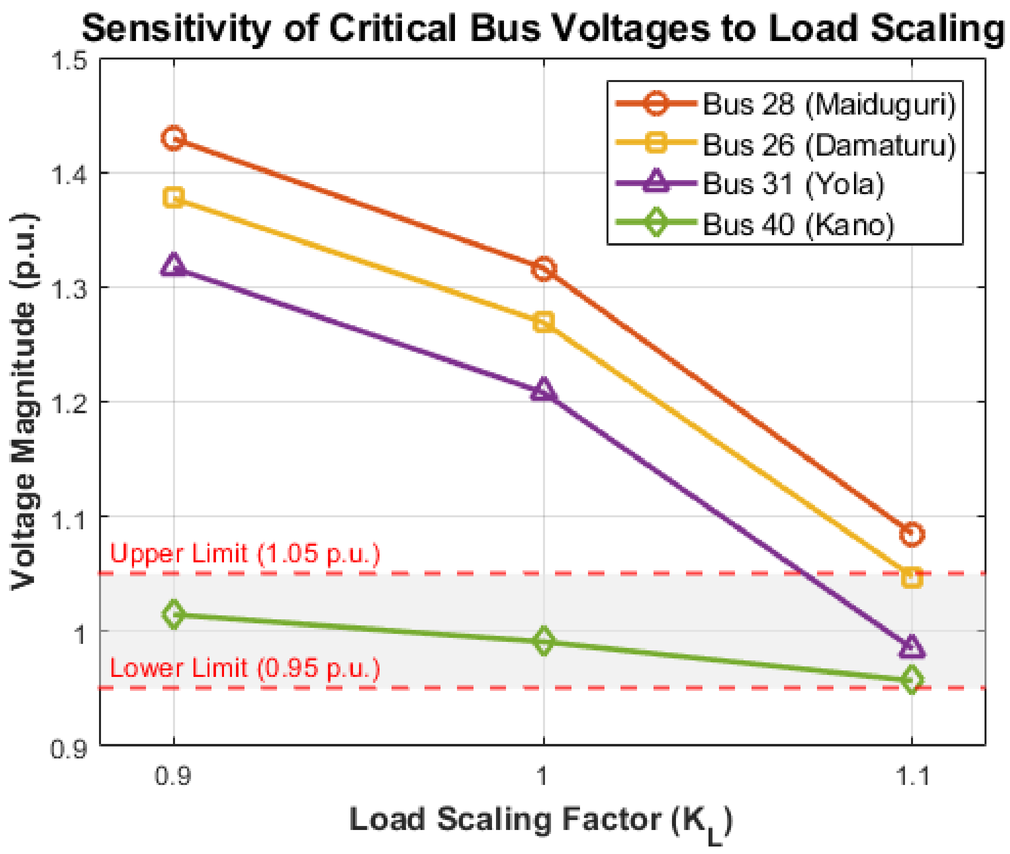

Figure 8: Bimodal Voltage Vulnerability Profile of Critical Buses Under Scaled Loading Conditions

This bimodal vulnerability demonstrates that the Nigerian grid faces distinct stability risks across its expected operating envelope: extreme capacitive charging overvoltages at light loads, and reactive power exhaustion leading to instability at heavy loads. This fundamentally underscores the necessity for dynamic reactive power compensation (such as STATCOMs) capable of both inductive absorption and capacitive injection, rather than fixed shunt devices.

3.5 N-1 Contingency Analysis

Of the 96 single-line contingencies evaluated, 88 resulted in NR convergence and 8 caused voltage collapse. The eight collapse-causing outages are Lines 1, 17, 18, 33, 45, 76, 91, and 92. Lines 17 and 76 are the two parallel circuits forming the Gombe–Jos corridor; loss of either alone collapses the North-East network. Lines 91 and 92 form the Calabar–Gombe segment. These eight lines represent absolute single points of failure in the network. Table 6 presents the top 10 converged N-1 contingencies ranked by maximum post-contingency FVSI, along with the four most severe collapse-inducing outages

Table 6: Top 10 N-1 Contingencies Ranked by Maximum FVSI and Selected Collapse Scenarios

Line Out	Active Power Loss (MW)	Critical Bus (Max L-Index)	Max FVSI	Max Lmn	Max LQP	System Status
Line 79	56.4	Bus 31 (0.7920)	0.9916	1.0011	1.2011	CONVERGED
Line 80	56.4	Bus 31 (0.7920)	0.9916	1.0011	1.2011	CONVERGED
Line 52	59.0	Bus 31 (0.6753)	0.9272	0.9328	1.1096	CONVERGED
Line 72	56.1	Bus 31 (0.6689)	0.9218	0.9271	1.1019	CONVERGED
Line 73	56.1	Bus 31 (0.6689)	0.9218	0.9271	1.1019	CONVERGED
Line 74	56.1	Bus 31 (0.6689)	0.9218	0.9271	1.1019	CONVERGED

Line 75	56.1	Bus 31 (0.6689)	0.9218	0.9271	1.1019	CONVERGED
Line 38	55.5	Bus 31 (0.6609)	0.9202	0.9254	1.0997	CONVERGED
Line 39	55.5	Bus 31 (0.6609)	0.9202	0.9254	1.0997	CONVERGED
Line 77	55.5	Bus 31 (0.6609)	0.9202	0.9253	1.0997	CONVERGED
Line 17	NaN	NaN	NaN	NaN	NaN	COLLAPSE
Line 76	NaN	NaN	NaN	NaN	NaN	COLLAPSE
Line 91	NaN	NaN	NaN	NaN	NaN	COLLAPSE
Line 92	NaN	NaN	NaN	NaN	NaN	COLLAPSE

Figure 9 visually interprets the severity of the network's structural fragility by plotting the Maximum Fast Voltage Stability Index (FVSI) for the top converged N-1 scenarios. The critical threshold for voltage collapse (FVSI = 1.0) is denoted by the dashed upper limit. The trend clearly isolates the Lafia–Jos parallel circuits (Lines 79 and 80) as severe structural anomalies within the broader grid context. While secondary contingencies elevate the system stress profile (FVSI ≈ 0.92), the isolated loss of either Line 79 or 80 abruptly spikes the index to 0.9916. This visual trend confirms that under peak stress, the North-Central transfer corridor operates with practically zero reactive stability margin, rendering it highly susceptible to cascading voltage collapse even before an N-2 event occurs.

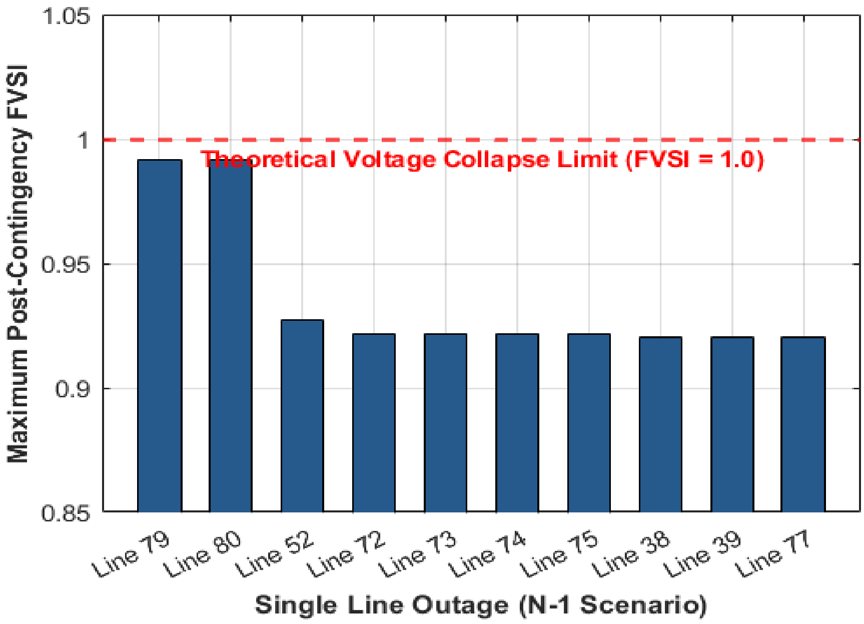

Figure 9: Proximity to Voltage Collapse: Maximum FVSI Profile for Top Converged N-1 Contingencies

3.6 N-2 Contingency Analysis

Table 7 presents the ten most severe N-2 contingencies evaluated in this study. To interpret the systemic threat posed by these dual outages, Figure 10 visualizes the Maximum Fast Voltage Stability Index (FVSI) for each scenario, applying a color-coded threshold at the theoretical voltage collapse limit (FVSI = 1.0). This graphical distinction clearly delineates between critical network stress (blue) and practical system failure (red).

Table 7: Top 10 N-2 Contingencies Ranked by Maximum FVSI

L1 & L2 Out	Active Power Loss (MW)	Critical Bus (Max L-Idx)	Max FVSI (Line)	Max Lmn (Line)	Max LQP (Line)	System Status
Line 19 & 79	59.0	Bus 31 (0.8826)	1.0174 (17)	1.0286 (17)	1.2381 (17)	Unstable / Practical Collapse
Line 19 & 80	59.0	Bus 31 (0.8826)	1.0174 (17)	1.0286 (17)	1.2381 (17)	Unstable / Practical Collapse
Line 20 & 79	59.0	Bus 31 (0.8826)	1.0174 (17)	1.0286 (17)	1.2381 (17)	Unstable / Practical Collapse
Line 20 & 80	59.0	Bus 31 (0.8826)	1.0174 (17)	1.0286 (17)	1.2381 (17)	Unstable / Practical Collapse
Line 52 & 79	59.1	Bus 31 (0.8101)	1.0046 (17)	1.0149 (17)	1.2197 (17)	Unstable / Practical Collapse
Line 52 & 80	59.1	Bus 31 (0.8101)	1.0046 (17)	1.0149 (17)	1.2197 (17)	Unstable / Practical Collapse
Line 72 & 79	56.8	Bus 31 (0.8032)	0.9986 (17)	1.0085 (17)	1.2110 (17)	Critically Stressed
Line 72 & 80	56.8	Bus 31 (0.8032)	0.9986 (17)	1.0085 (17)	1.2110 (17)	Critically Stressed
Line 73 & 79	56.8	Bus 31 (0.8032)	0.9986 (17)	1.0085 (17)	1.2110 (17)	Critically Stressed
Line 73 & 80	56.8	Bus 31 (0.8032)	0.9986 (17)	1.0085 (17)	1.2110 (17)	Critically Stressed

The simulation reveals a critical phenomenon: the synergistic outage of Line 19 and Line 79 (or their parallel equivalents, Lines 20 and 80) produces a maximum FVSI of 1.0174 on Line 17 (Gombe–Jos). Because an FVSI exceeding unity dictates a total exhaustion of reactive power transfer capability, these specific top-ranked combinations push the system beyond its physical stability boundary. Thus, they represent practical voltage collapse scenarios, even though the Newton-Raphson algorithm achieved numerical convergence.

A key pattern in the N-2 results as seen in Figure 10, is that every single top-ranked dual contingency involves either Line 79 or Line 80. This graphically and mathematically confirms that the Lafia–Jos corridor operates as the absolute lynchpin of the North-Central grid, lacking the redundancy to survive compounded failures. Furthermore, Bus 31 (Yola) consistently records the highest post-contingency L-index across all top N-2 scenarios (reaching 0.8826 in the worst-case), confirming its severe structural vulnerability to upstream outages.

The synergistic failure of these transmission pairs reveals that the loss of the Lafia–Jos circuit, compounded by the loss of a secondary supporting corridor, exposes the entire North-Central zone to immediate collapse conditions. The economic implications are substantial: the estimated costs of such unplanned, system-wide outages far exceed the localized investment required for dynamic reactive power compensation and corridor reinforcement.3.7 Techno-Economic Implications of Grid Vulnerability.

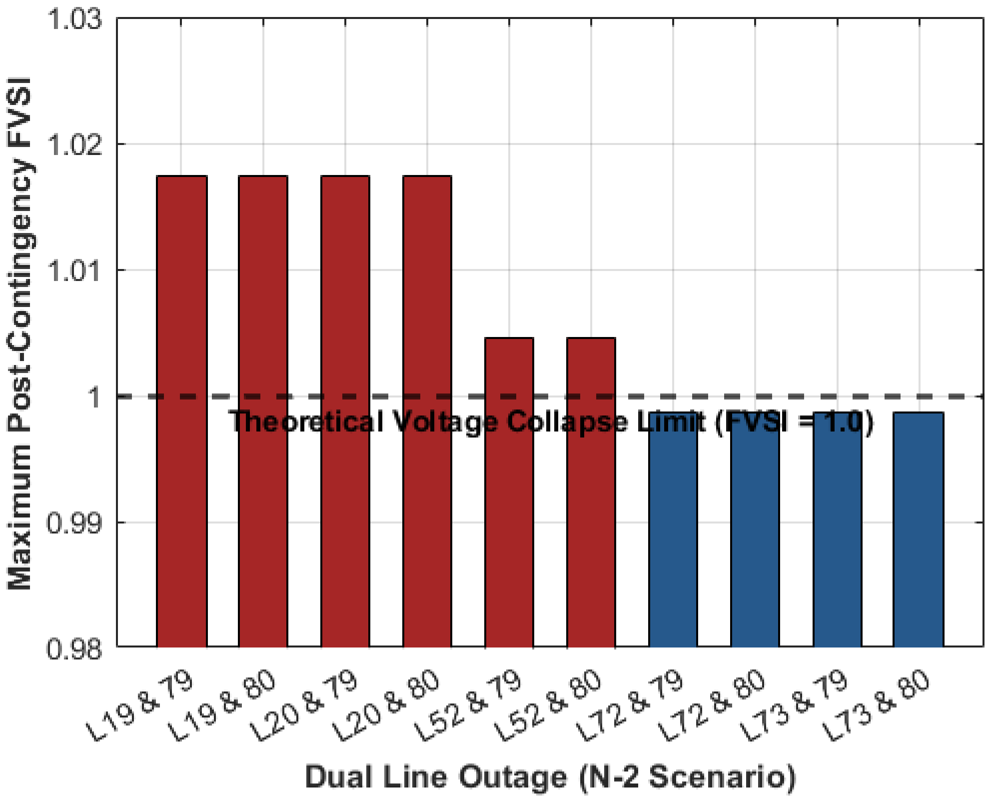

Figure 10: Practical Voltage Collapse vs. Critical Stress: Color-coded maximum FVSI profile demonstrating index values breaching the unity stability threshold (FVSI > 1.0) under severe N-2 contingencies

The severe structural fragilities identified in the steady-state and contingency analyses translate directly into massive financial deficits for both utility providers and consumers. To justify the capital expenditure required for dynamic reactive power compensation (FACTS), the technical vulnerabilities of the 330 kV network must be evaluated through an economic lens.

1. **Cost of Continuous Active Power Loss:** Under normal base-case operating conditions, the fully corrected network simulation revealed a continuous active power loss of 55.54 MW. Utilizing the Service Reflective Tariff of 209.50 NGN/kWh applicable to commercial and high-demand consumers (Eko Electricity Distribution Company [EKEDC], 2020), this steady-state inefficiency carries a severe financial penalty. Converting the tariff to wholesale megawatt-hours (209.500 NGN/MWh), the annual cost of uncompensated power loss (S_{loss}) is formulated as equation (16):

$$S_{loss} = P_{loss} \times 8760 \times C_{energy}$$

Where; P_{loss} is the simulated 55.54 MW loss, 8760 represents total annual operating hours, and C_{energy} is the energy tariff. This equates to an annual revenue drain of approximately 101.99 billion NGN. The strategic deployment of FACTS devices to optimize power flow and reduce these losses provides a direct mechanism for capital recovery.

2. **Macroeconomic Cost of System Collapse:** Beyond steady-state losses, the N-1 and N-2 contingency analyses identified multiple absolute points of failure (e.g., the synergistic loss of the Lafia–Jos (Line 79) and Kaduna–Shiroro (Line 19)) that plunge the network into practical voltage collapse. The economic damage of these sudden blackouts is catastrophic. Adeoye (2023) estimates that a single hour of total national grid collapse incurs losses of approximately 1.125 billion NGN for domestic consumers alone, severely crippling utility revenue generation and maintenance capabilities. Furthermore, Ogunmakinde et al. (2024) demonstrated that a mere 1% increase in power outage duration corresponds to a 2.86% decline in regional GDP, translating to billions of dollars in macroeconomic loss.

3. **Environmental and Public Health Externalities:** Beyond direct financial deficits, the chronic instability of the grid forces consumers to rely heavily on self-generated power, introducing severe environmental and public health externalities. To cope with the frequent collapses of vulnerable transmission corridors, both households and Small and Medium Enterprises (SMEs) resort to inefficient diesel and petrol generators. This widespread proliferation not only consumes an estimated $23 billion in fuel annually (Ogunmakinde et al., 2024) but also emits substantial greenhouse gases and toxic particulate matter. The resulting noise and air pollution severely degrade local air quality, introduce significant health risks to the population, and contradict national sustainable development goals (Owosho, 2025). Consequently, stabilizing the grid via dynamic compensation yields a critical environmental dividend by directly reducing the nation's dependency on high-emission backup generation.

4. **Regional Impact on the North-East:** The burden of grid instability is not distributed equally. As demonstrated in Section 3.2, the Northern transmission corridors—specifically Maiduguri (Bus 28), Damaturu (Bus 26), and Yola (Bus 31)—exhibit the most severe Ferranti-driven overvoltages and highest collapse proximities. Owosho (2025) empirically established that in the North-East region, such frequent outages increase operational costs for Small and Medium Enterprises (SMEs) by up to 46% due to heavy reliance on expensive backup generators, subsequently driving a 50% loss in productivity.

Consequently, mitigating voltage violations at these specific Northern nodes via dynamic STATCOM or TCSC deployment is not merely a grid code compliance requirement; it is a critical regional economic imperative. The subsequent optimization phase of this research (e.g., GA-MPSO) must therefore utilize a multi-objective fitness function that minimizes the annualized capital cost of FACTS installations while maximizing the monetization of saved active power losses and averted blackout penalties.

3.8 PandaPower Cross-Validation

To ensure mathematical robustness, the base-case Newton-Raphson (NR) load flow was independently cross-validated using PandaPower on the corrected 50-bus network model. The comparative analysis demonstrated high precision between the two simulation environments. Bus voltage magnitudes and stability indices matched the primary MATPOWER implementation to within 0.0005 p.u. (e.g., the critical L-index at Bus 31 recorded 0.6603 in MATPOWER versus 0.6605 in PandaPower). Furthermore, total system active power losses matched to within 0.05 MW (55.54 MW versus 55.51 MW, respectively). This stringent cross-platform validation—largely absent in prior 50-bus Nigerian grid literature—confirms that the severe voltage violations and stability risks observed are inherent characteristics of the physical network topology, rather than algorithmic artifacts of a single software environment.

4.0 Conclusion

This study delivered a rigorous, multiply-validated steady-state and contingency assessment of the Nigerian 330 kV, 50-bus transmission network. The principal findings, framed within the verified constraints of the modeled system, are as follows:

1. **Geospatial Validation:** Geospatial verification utilizing the Haversine formula confirms that the Fakun–Kainji 330 kV transmission corridor (Bus 34 to Bus 50) spans approximately 501–562 m, corroborating the published value of ~0.50 km. As these substations are co-located near the Kainji Dam, this parameter is physically accurate. This exercise demonstrates the necessity of integrating GPS-corroborated geospatial tools when validating Nigerian grid datasets.

2. **Dataset Correction:** A systematic mathematical error in recently published shunt susceptance data was identified and rectified. The published B values erroneously corresponded to series branch admittance (X/(R2+X2)) rather than physical shunt charging susceptance. Applied uniformly across all 96 branches, this correction eliminated non-physical reactive power injections, successfully stabilized the Jacobian matrix, and yielded a physically consistent base-case active power loss of 55.54 MW.

3. **Base-Case Voltage Violations:** Five critical Northern buses exhibit severe Ferranti-driven overvoltages: Maiduguri/Bus 28 (1.3166 p.u.), Damaturu/Bus 26 (1.2694 p.u.), Yola/Bus 31 (1.2082 p.u., maximum system L-index of 0.6603), Gombe/Bus 27 (1.2005 p.u.), and Jos/Bus 30 (1.1096 p.u.). Derived from a fully corrected and cross-validated dataset, these findings precisely quantify grid vulnerability beyond prior literature reports.

4. **Bimodal Operational Vulnerability:** Load sensitivity analysis ($KL \in \{0.9, 1.0, 1.1\}$) reveals a dual-threat stability profile. Ferranti-driven overvoltages severely intensify under light load conditions ($KL=0.9$),

peaking at nearly 1.43 p.u. Conversely, heavy load conditions (KL=1.1) drive Bus 31 (Yola) into theoretical voltage collapse, with its L-index surging to 1.0612. This bimodal vulnerability definitively proves the operational necessity for dynamic, rather than fixed, reactive power compensation.

5. **Structural Fragility**: The N-1 contingency analysis identified 8 single transmission lines that act as absolute points of failure, causing immediate system collapse upon individual removal. Furthermore, the N-2 analysis isolated the Lafia–Jos corridor (Lines 79 and 80) as the system's most critical transmission axis. The simultaneous outage of Lines 19 and 79 produces a maximum FVSI of 1.0174, indicating a state of practical voltage collapse despite mathematical solver convergence.

These findings are strictly specific to the modeled steady-state operating conditions and validated load profiles. The established vulnerabilities provide a robust, mathematically verified foundation for future research into the optimized placement and sizing of hybrid FACTS devices to secure the Nigerian grid.

5.0 Recommendation

Based on the validated stability assessment of the Nigerian 330 kV transmission network, the following strategic interventions are recommended:

1. **Dynamic Reactive Power Compensation:** The immediate deployment of dynamic reactive compensation—specifically STATCOM or SVC devices—at Maiduguri (Bus 28) and Damaturu (Bus 26) is critical. While traditional fixed shunt reactors can suppress Ferranti-driven overvoltages during light loading (Udo & Aminu, 2019; Foqha et al., 2023), the bimodal vulnerability of the network necessitates dynamic devices capable of providing fluid inductive and capacitive support across the entire operating envelope (Yarlagadda et al., 2022).

2. **Corridor Reinforcement:** The Lafia–Jos transmission axis (Lines 79 and 80) must be prioritized for physical or systemic reinforcement. Installing a third parallel circuit or deploying Thyristor Controlled Series Capacitors (TCSC) for active power flow control will directly mitigate the severe N-1 and N-2 stability bottlenecks identified in the contingency analysis. This intervention is critical because the current Lafia–Jos corridor operates with near-zero effective redundancy, representing the system’s single greatest reliability risk to the Northern zones.

3. **Institutionalization of Geospatial Auditing:** The Transmission Company of Nigeria (TCN) should institutionalize GPS-corroborated verification of all transmission line length parameters within its operational planning datasets. Mandating geospatial validation as a standard protocol, as demonstrated in this study, will eliminate the propagation of systematic impedance modeling errors.

4. **Future Research Directions:** Future studies should focus on the optimal, coordinated placement and sizing of hybrid FACTS devices (STATCOM and TCSC) across the grid. Executing advanced metaheuristic optimization techniques, such as Genetic Algorithm-Modified Particle Swarm Optimization (GA-MPSO), on the fully corrected and cross-validated base-case model established in this work will yield highly reliable deployment strategies.

Acknowledgments

I wish to express my profound gratitude to God for His grace and enablement throughout the duration of this research. My sincere appreciation goes to my family for their unwavering encouragement and support during the course of this work.

I am particularly indebted to my supervisor, Dr. Chibueze Kingsley Obute, whose expert ideas, recommendations, and technical assistance contributed greatly to the success of this research. I also acknowledge the Department of Electrical Engineering, Nnamdi Azikiwe University, for providing the institutional support necessary to complete this study.

Nomenclature

a = Intermediate Haversine parameter

B_{series} = Series branch susceptance (S)

B_{shunt} = Shunt charging susceptance (S)

c = Central angle (radians)

C_0 = Nominal capacitance per unit length (nF/km)

d = Great-circle distance (km)

I_{ij} = Current flow between bus i and bus j (A)

K_L = Load scaling factor

L_j = L-index of load bus j

P_D = Total active power demand (MW)

P_G = Total active power generation (MW)

P_{loss} = Total active power loss (MW)

Q_j = Reactive power injection at bus j (MVAr)

R_E = Mean radius of the Earth (km)

R_{ij} = Series resistance of branch ij (Ω)

V_i = Voltage magnitude at bus i (pu)

X_{ij} = Series reactance of branch ij (Ω)

Y_{bus} = Bus admittance matrix

Z_{ij} = Impedance of branch ij (Ω)

Δϕ = Latitude difference (radians)

Δλ = Longitude difference (radians)

θ = Voltage angle (degrees)

ω = Angular system frequency (rad/s)

Declaration of Generative AI and AI-assisted technologies in the writing process

During the preparation of this work, the author(s) used software and AI tools (e.g., Gemini) to source information, find related materials, and generate figures. After using these tools, the author(s) reviewed and edited the content as needed and take(s) full responsibility for the final version of this publication.

References

Adeoye, O.S. 2023. Power grid collapse impacts on consumers and utility companies in Nigeria. *Global Journal of Engineering and Technology*, 2(6), pp. 1–7.

Ekanem, N., Umoren, M. and Udofia, K. 2025. Reinforcement learning-assisted voltage stability analysis of the Nigerian power grid using DVR and BESS. *Journal of Engineering Research and Reports*, 27(6), pp. 286–304. Available from: https://doi.org/10.9734/jerr/2025/v27i61545.

Ekong, K.K. 2022. *Power-voltage and reactive-voltage curves for voltage stability analysis on the 58-bus, 330 kV Nigerian network*. Unpublished master's dissertation, Covenant University, Ota, Nigeria.

Eko Electricity Distribution Company (EKEDC). 2020. *Service reflective tariff*. Available from: https://www.ekedp.com/tariff-plans **[Accessed 19 November 2025]**.

Ezeruigbo, E.N., Ekwue, A.O. and Anih, L.U. 2021. Voltage stability analysis of Nigerian 330 kV power grid using static PV plots. *Nigerian Journal of Technology*, 40(1), pp. 70–80.

Foqha, T., Alsadi, S., Refaat, S.S. and Abdulmawjood, K. 2023. Experimental validation of a mitigation method of Ferranti effect in transmission line. *IEEE Access*, 11, pp. 15878–15895.

Geregu Power Plc. 2022. *Investor presentation*. Available from: https://prjdg-unstruc.s3.ca-central-1.amazonaws.com/Others/News/5641e693-0537-41c4-ab7d-29084470508d **[Accessed 19 November 2025]**.

Google Maps. 2026. *Satellite imagery: Kainji Dam area, Niger State, Nigeria*. Available from: https://maps.google.com **[Accessed 24 Feburary 2026]**.

Grainger, J.J. and Stevenson, W.D. 1994. *Power system analysis*. New York: McGraw-Hill.

Kundur, P. 1994. *Power system stability and control*. New York: McGraw-Hill.

Moghavvemi, M. and Jasmon, G.B. 1997. New method for indicating voltage stability condition in power system. In: *Proceedings of the third international power engineering conference*, Singapore, pp. 223–227.

Nkan, I.E., Okoro, O.I., Awah, C.C. and Akuru, U.B. 2019. Investigating the steady state stability of the Nigerian 48-bus system using FACTS devices. *Nigerian Journal of Technology*, 38(3), pp. 732–739. Available from: https://doi.org/10.4314/njt.v38i3.27.

Obasi, R., Okonkwo, I. and Obinwa, C. 2025. Voltage stability enhancement of Nigeria 330 kV grid using UPFC, FACTS, ANN and PSO. *International Journal of Innovative Research in Engineering and Management*, 12(4), pp. 30–38. Available from: https://doi.org/10.55524/ijirem.2025.12.4.6.

Ogunwuyi, O.J., Adio, M.O., Olushola, I.B., Bisiriyu, A.O. and Bamkefa, I.A. 2024. Evaluation of economic consequences of the Nigeria national grid collapse. *Adeleke University Journal of Engineering and Technology*, 7(1), pp. 163–167.

Okampo, E.J., Nwulu, N.I. and Bokoro, P.N. 2022. Optimization of voltage security with placement of FACTS device using modified Newton-Raphson approach: a case study of the Nigerian transmission network. *Energies*, 15(12), p. 4211. Available from: https://doi.org/10.3390/en15124211.

Olabisi, P.O. and Ayeni, G. 2023. Voltage quality analysis on power transmission networks: a case study of 330 kV power transmission network in Nigeria. *Journal of Engineering Research and Reports*, 25(4), pp. 42–50.

Onyegbadue, I.A., Ukagu, S.N. and Okonkwo, D.O. 2024. Voltage stability assessment of Nigeria 330 kV power grid: a critical bus perspective. *UNIZIK Journal of Engineering and Applied Sciences*, 3(5), pp. 1382–1401. Available from: https://journals.unizik.edu.ng/ujeas/article/view/4988/4109 **[Accessed 20 October 2025]**.

Owosho, S.D. 2025. Evaluating the economic impact of frequent power outages on Nigeria's national grid: a case study of North-East Nigeria. *Scholarly Journal of Science and Technology Research and Development*, 4(5), pp. 1–22. Available from: https://doi.org/10.5281/zenodo.17843086.

Saadat, H. 2010. *Power system analysis*. 3rd ed. Alexandria: PSA Publishing.

Samuel, I., Katende, J., Awosope, C., Awelewa, A., Adekitan, A. and Agbetuyi, A. 2019. Power system voltage collapse prediction using NLSI-1: a case study of the 330 kV Nigerian national grid. *International Journal of Electrical and Computer Engineering*, 9(6), pp. 5125–5133. Available from: https://doi.org/10.11591/ijece.v9i6.pp5125-5133.

Sobayo, A., Adejumobi, O., Adebisi, I. and Adams, D. 2024. Contingency approach for static security assessment on the Nigerian 330 kV electric power transmission grid. *Advances in Science and Technology*, 154, pp. 203–212. Available from: https://doi.org/10.4028/p-stvce4.

Thurner, L., Scheidler, A., Schäfer, F., Menke, J.H., Dollichon, J., Meier, F., Meinecke, S. and Braun, M. 2018. Pandapower: an open-source Python tool for convenient modeling, analysis and optimization of electric power systems. *IEEE Transactions on Power Systems*, 33(6), pp. 6510–6521. Available from: https://doi.org/10.1109/TPWRS.2018.2829021.

Transmission Company of Nigeria. 2020. *Grid operations report*. Abuja: TCN.

Udo, J.F. and Aminu, M.A. 2019. Transient stability improvement on Jos–Gombe 330 kV line using static var compensator. *Journal of Scientific Research and Reports*, 24(5), pp. 1–7.

Ugwuanyi, N.S., Ozioko, I.O. and Ugwuoke, N.C. 2024. *Dataset for the Nigerian 50-bus 330 kV power grid*. Available from: https://doi.org/10.5281/zenodo.12091189 **[Accessed 10 May 2025]**.

Yarlagadda, V., Lakshminarayana, G., Ambati, G., Nireekshana, T. and Karthika, G.A. 2022. Mitigation of Ferranti effect and voltage control in transmission systems using fuzzy logic controlled SVC. In: *Proceedings of the international conference on smart technologies and systems for next generation computing (ICSTSN)*, pp. 1–6.